Effect of Al on the columnar-to-equiaxed transition for Ti-6%Al and Ti-45%Al by cellular automaton

Min Zhang*, Yulan Zhou, Qin Xue, Jihong Li, Erlong and Mu

Department of Material Shaping and Control, School of Materials Science and Engineering, Xi'an University of Technology, NO.5 South Jinhua Road, Xi'an 710048, China

*Corresponding author

DOI: 10.5185/amlett.2018.1904
www.vbripress.com/aml

Abstract

A dendritic growth model is established by combining the physical properties of dendritic growth with the characteristics of the cellular automaton (CA) method. The heat process and the molten pool model of the arc-shaped in the process of welding solidification are coupled by using the interpolation method. On the basis of that, the growth of dendrites in the molten pool for Ti-6%Al and Ti-45%Al alloys is simulated and the influence of aluminium content on the morphology of dendrites in the welding solidification process is analysed. And also the microstructural evolution of the molten pool during the solidification process is implemented under the condition of the non-uniform temperature field. The results indicate that the temperature presents the gradual distribution in the non-uniform temperature field and the microstructure grows competitively at the center of the molten pool. During the progress of solidification, the solute atoms are enriched in between dendrite arms with the segregation of solute. Simultaneously, with the change of temperature field, the morphology of dendrites has asymmetry. In addition, the columnar crystals are largely converted to equiaxed crystals for Ti-6%Al alloy while the result is the opposite for Ti-45%Al alloy resulting from the change of the aluminium content. The simulated results are in good agreement with the experimental ones. Copyright © 2018 VBRI Press.

Keywords: Cellular automaton, dendritic distribution, solute concentration, welding heat process.

Introduction

The increasing demands for aircraft and aerospace system performance have extremely called for the development of improved structural materials. Ti-Al alloy currently attracts people's wide attention owing to its low density, high strength, good corrosion resistance, and heat resistance, which has been widely used in aerospace and automotive field **[1-3]**. In addition, its high aluminum content makes it highly resistant to oxidation **[4]**. But it will produce a larger molten pool under the condition of the incorrect welding parameters is mainly due to its high melting point and poor thermal conductivity. This can lead to the solidification time after welding becoming longer and the grain becoming relatively larger with resulting in brittle welded joints **[5]**. Therefore, based on the experimental real-time observation, it is difficult to detect the microstructure evolution during solidification.

With the rapid development of computer technology and computational materials science, the calculation of macroscopic temperature field and stress field has become increasingly mature **[6-7]**, which makes the simulation of microstructure evolution possible. In the last 20 years, the simulation of dendritic growth in solidification process was carried out by various numerical computation models. The two-dimensional dendritic growth model was firstly built based on the CA method by Gandin and Rappaz **[8]**, combined with non-uniform nucleation and dendritic growth theory, the dendritic growth in solidification process was simulated. On the basis of the finite element method and cellular automata technology, the growth morphology of columnar crystals in the molten pool was simulated **[9-11]**. Tan *et. al.* **[12-13]** combined the CA method **[14-15]** with phase field (PF) method **[16-17]**, the growth morphology of dendrites in macro and micro fields was predicted by means of the two-dimensional CA-PF model. Compared with casting, the volume of molten pool is smaller with non-uniform temperature distribution, while the solidification speed of liquid metals is very fast, and the metal of molten pool is in the overheated state with large temperature gradient. These characteristics mentioned above make the numerical simulation for the process of the molten pool solidification has irreplaceable particularity. The solidification process of the welding molten pool was investigated by using CA-FD coupled model **[18]**. However, the numerical simulation investigation for columnar-to-equiaxed transition (CET) of Ti-Al alloys

during solidification processes of the welding molten pool is relatively less.

In view of the above problems, the CA model of dendrite growth of thermal solidification is applied to the welding thermal process model, the semi-arc and arc-shaped pool model of dendritic growth were obtained. Based on the models established, the evolution of dendritic morphology on the CET in the molten pool is theoretically and experimentally investigated under the condition of the change of Al initial composition for Ti-Al alloys. And the distribution of solute concentration in the process of dendritic growth is analyzed. The experiments are presented and discussed.

Mathematical model and numerical algorithm

Model hypothesis

In order to better describe dendritic growth behavior, the thermal diffusion, solute diffusion, interface energy and the dynamic response of high-speed growth must be comprehensively considered. Hence, there is a need to make basic assumptions about the used model **[19]**.

1) When the undercooling is not large, the dynamic effect at high growth is not taken into account and the diffusion of solute in the solid phase is neglected.
2) The flow of the melt is neglected and the interface is always in equilibrium, simultaneously, both sides of the interface need to be met the relationship as follows:

$$C_s = k_0 C_l \tag{1}$$

where C_s is the solid phase solute concentration at the interface, while C_l is the liquid phase solute concentration at the interface, k_0 is the balanced distribution coefficient.

Temperature field model

The establishment of the heat source model and the simulation of the welding temperature field play an important role on the welding numerical simulation. According to the previous experience, the calculated results of Gaussian heat source distribution are in good agreement with the actual welding process. In the welding process, the heat transfer from the arc heat source to the weldment through a certain area which is called heating spots. The heating spots have uneven heat distribution, i.e., the edge is few while the center is more. The Gaussian function is used to approximately describe the heat flux distribution on the heated spot. The heat flux at the distance from the center of the heated spot can be expressed as **[20]**:

$$q_r = q_m \exp\left(\frac{-3r^2}{r_h^2}\right) \tag{2}$$

Where q_m is the maximum heat flux at the center of the heated spot in $J/(m^2.s)$, r is the direct distance from the arc heating spot in *mm*, r_h, is effective radius of arc in *mm*. The effective radius of arc r_h is related to thermal concentration factor K, i.e., $K = 3/r_h^2$ and its value is used to represent the degree of concentration of heat flow. In the simulation process, the moving gauss heat source model is derived as:

$$q_r = \frac{q_m}{h}\exp\left[-\frac{(3(x-v\Delta t)^2 + y^2)}{r_h^{\,2}}\right] \tag{3}$$

where h is the thickness of the weldment in *mm*, v is the moving speed of welding heat source in *m/s*, and Δt is the time step in *s*.

In order to accurately simulate the solidification process of the molten pool, it is extremely necessary to consider the convective heat transfer behavior of the liquid metal in the molten pool and the thermal process of the external solid region of the molten pool. Therefore, the fluid flow process is more complex. In order to simplify the calculation and facilitate the practical application, the heat conduction problem of arc welding is considered while the convective heat transfer is neglected in the welding process. Then, the two-dimensional transient thermal equation is obtained as **[21]**:

$$\rho C_{\mathrm{p}} \frac{\partial T}{\partial t} = \lambda\left(\frac{\partial^2 T}{\partial \mathrm{x}^2} + \frac{\partial^2 T}{\partial y^2}\right) + q_r \tag{4}$$

where ρ is density in $kg \cdot m^{-3}$, C_p is volume specific heat capacity in $J \cdot m^{-3} \cdot K^{-1}$, λ is thermal conductivity in $W \cdot m^{-1} \cdot K^{-1}$.

The undercooled melt temperature can be derived by explicit difference for the equation (4):

$$T_{i,j}^{n+1} = \frac{\alpha \Delta t}{\Delta x^2}\left(T_{i+1,j}^n + T_{i-1,j}^n + T_{i,j+1}^n + T_{i,j-1}^n - 4T_{i,j}^n\right) + T_{i,j}^n \tag{5}$$

where α is the thermal diffusivity in m^2/s, Δt is the time step in *s*, Δx is the grid size in *mm*.

Dendrite growth model

In the CA model, the undercooling of the liquid-solid interface mainly includes temperature, concentration and curvature **[22]**. The anisotropy of the interface energy has great effect on the curvature undercooling, so the model must consider the interface anisotropy. At the time t_n, the degree of undercooling in the solid-liquid interface prerequisite is calculated as **[23-25]:**

$$\Delta T(t_n) = T' - T_{i,j} + m_L(C_0 - C_L^*) + \Gamma K(t_n)\left\{1 - 15G_x \cos\left[4(\theta - \theta_0)\right]\right\} \tag{6}$$

where T' is the temperature at the interface, $T_{i,j}$ is the temperature of the undercooled melt. C_0 is initial solute concentration, C_L^* is the solute concentration of the liquid at the interface, and m_L is the slope of the

Copyright © 2018 VBRI Press

liquidus. Besides, Γ is the Gibbs-Thompson coefficient, $K(t_n)$ is the interface curvature which calculated from Eq.(7), G_x is anisotropy intensity of the liquid-solid interface. θ_0 is the angle between the growth direction of the dendrites and the positive direction of the coordinate axes which is calculated from Eq.(8), while θ is the angle between the normal of the solid/liquid interface and the positive direction of the coordinate axis, which is calculated from Eq.(9).

$$K(t_n)=\left[2\frac{\partial f_s}{\partial x}\frac{\partial f_s}{\partial y}\frac{\partial^2 f_s}{\partial x\partial y}-\frac{\partial^2 f_s}{\partial x^2}\left(\frac{\partial f_s}{\partial y}\right)^2-\frac{\partial^2 f_s}{\partial y^2}\left(\frac{\partial f_s}{\partial x}\right)^2\right]\left[\left(\frac{\partial f_s}{\partial x}\right)^2+\left(\frac{\partial f_s}{\partial y}\right)^2\right]^{-3/2} \quad (7)$$

$$\theta_0=\cos^{-1}\left(\frac{\partial f_s/\partial x}{\left((\partial f_s/\partial x)^2+(\partial f_s/\partial y)^2\right)^{1/2}}\right) \quad (8)$$

$$\theta=\arctan\left(\frac{\partial f_s/\partial y}{\partial f_s/\partial x}\right) \quad (9)$$

In order to ensure stability in the explicit calculation of the composition field and the rate of advance of the solid-liquid interface, the time-step is determined by the following equation **[26]**:

$$\Delta t\le\frac{1}{5}\min\left(\frac{\Delta x^2}{D_l},\frac{\Delta x}{V_{\max}}\right) \quad (10)$$

where Δx is the grid size, D_l is solute diffusion coefficient in the liquid, and V_{max} represents the welding speed.

Coupling of dendritic growth and welding thermal processes

In the actual molten pool, the temperature in the same time is unequal at different positions. For simulating the process of dendrites growth in the molten pool, the welding temperature field and the CA model of dendritic growth are coupled during the solidification process. Besides, the relationship of temperature changes in the weld interface and the dendritic growth process are discussed. Due to the temperature field is macroscopic while dendritic growth is microscopic, hence, it is required that the obtained macroscopic unit temperature is converted into the microscopic unit temperature. Then, the temperature of the microscopic unit is obtained by using the interpolation formula. The interpolation formula can be expressed as **[27]**:

$$T=\sum_{i=1}^{N}L_i^{-1}T_i/\sum_{i=1}^{N}L_i^{-1} \quad (11)$$

where T is the temperature of microscopic grid in ℃, T_i is the macroscopic unit temperature around the microscopic grid in ℃, and L_i is the distance from the microscopic grid to the surrounding macro element in *mm*.

During the simulation process, it is very necessary to firstly determine the location of the fusion line in the molten pool. The fusion line contributes to decide the calculated area for the simulated dendritic growth. However, the actual shape of the molten pool is an irregular circular boundary, which is controlled by various factors such as the welding line energy, work-piece thickness and thermal conductivity of the work-piece etc. For the purpose of approximating the simplified actual model, therefore, an ideal model is established by setting the radius of molten pool and assuming that the shape of molten pool remains the same during solidification. The distance from any cell to the nucleation core can be derived by the following equation:

$$R(i,j)^2=(i-i_0)^2+(j-\frac{j_0}{2})^2 \quad (12)$$

where R is the distance from the welding arc to the heat source center in *mm; i, j* are used to represent the horizontal and vertical coordinates in the simulation area, respectively.

The thermo-physical properties of Ti Al alloys used in this research work are shown in the **Table. 1** and **Table 2**.

Table 1. The thermo-physical properties of Ti-45%Al used in this work.

Parameters	value
Liquidus temperature , T_L (K)	1830
Liquidus slope, m_L ($at.\%$)	-7.9
Equilibrium partition coefficient, k_0	0.78
Gibbs-Thompson coefficient, Γ ($K\cdot m$)	2.4E-7
Solute diffusion coefficient in the liquid, D_l (m^2/s)	3E-9
Alloy initial composition, C_0 ($at.\%$)	45
Welding thermal efficiency, η	0.75
Energy concentration factor, K ($1/m^2$)	5
Surrounding medium temperature, T_f (K)	297

Table 2. The thermo-physical properties of Ti-6%Al used in this work.

Parameters	value
Liquidus temperature, T_L (K)	1900
Liquidus slope, m_L ($at.\%$)	-9.375
Equilibrium partition coefficient, k_0	0.55
Gibbs-Thompson coefficient, Γ ($K\cdot m$)	1.5E-7
Solute diffusion coefficient in the liquid, D_l (m^2/s)	5E-5
Alloy initial composition, C_0 ($at.\%$)	6
Welding thermal efficiency, η	0.75
Energy concentration factor, K ($1/m^2$)	5
Surrounding medium temperature, T_f (K)	297

Copyright © 2018 VBRI Press

Experimental

To verify the accuracy of the simulated results, the base materials used in welding test are 5 mm thick Ti-6% Al alloy and Ti-45%Al alloy plate. The specimens were mechanically ground with 120-grit SiC paper. Then pickled in a solution composed of 400mLH_2O+40gKOH+40mLH_2O_2 and removed oil in 500mL acetone, finally purged with an ultrasonic cleaner in order to remove surface contaminants. TIG welding is the most commonly used method for titanium and its alloys, which is an excellent way to connect the sheet and the bottom of the welding. Therefore, gas tungsten-arc argon weld is produced manually and the welding method is self-fluxing on specimens of Ti-Al alloy plate. All welding are performed inside a weld room that was purified with carbon dioxide for 10 min prior to welding. The welding parameters are described as:

- current is 90A,
- voltage is 13.8V,
- and travel rate is 2mm/s.

Metallographic sections orientated transverse to the travel direction are cut from the welded samples. In order to obtain the metallographic microstructure, the inverted metallographic microscope GX671 is used.

Results and discussion

In order to better distinguish the shape of molten pool between the Ti-6%Al alloy and the Ti-45%Al alloy, the calculation area is divided into 10×20 rectangular macroscopic grids composed of 20×20 uniform microscopic grid for Ti-45%Al while it is divided into 20 × 20 rectangular macroscopic grids composed of 20×20 uniform microscopic grid for Ti-6%Al. In addition, the grid size is 5μm and the time step is 0.5ms, the number of iterations is 3000CAS, respectively.

The micro-temperature field distribution of the weldment

According to the **Fig. 1,** it can be seen that the welding molten pool appeared likes arc-shaped. At the initial stage of solidification, the entire pool is overheated and the nucleation is not yet begun. The temperature of the heat source is close to the melting point of the alloy.

And the temperature of molten pool center is the highest, successively reduced from the center to the edge. So when close to the edge of the molten pool, the heat scattered is faster with the priority to reach the nucleation conditions.

The dendritic growth of molten pool

In order to further study the dendrite evolution of the weld pool under the non-uniform temperature field, the dendritic morphology of Ti-6%Al alloy and Ti-45%Al alloy in the molten pool is analyzed. When the columnar crystals meet the equiaxed grains, as shown in **Fig. 2**, the growth of the columnar crystals will be hindered by the growth of the central equiaxed grains. It leads to prevent the vertical growth of the part columnar crystals while the horizontal growth is intensified and the secondary dendrite arm also is intensified, which finally achieves the transformation from the columnar crystals to the equiaxed crystals. The growth of the dendrites in the molten pool after the coupled welding temperature field also follows the respective growth rules, but exhibits randomness and symmetry. The number of columnar crystals is less than equiaxed crystals in molten pool of Ti-6%Al alloy while the number of equiaxed crystals is less than columnar crystals of Ti-45%Al alloy after the CET is over. Therefore, it can be seen that Al initial content in Ti-Al alloys has a great influence on dendritic morphology.

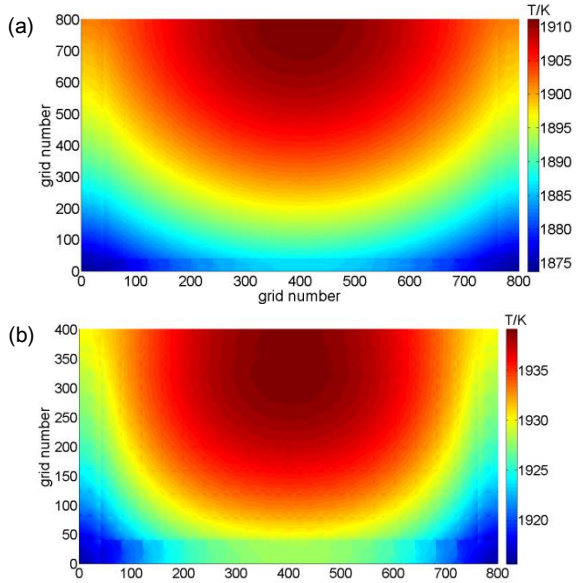

Fig. 1. The micro-temperature field distribution of the weld, (a) Ti-6%Al, (b) Ti-45%Al.

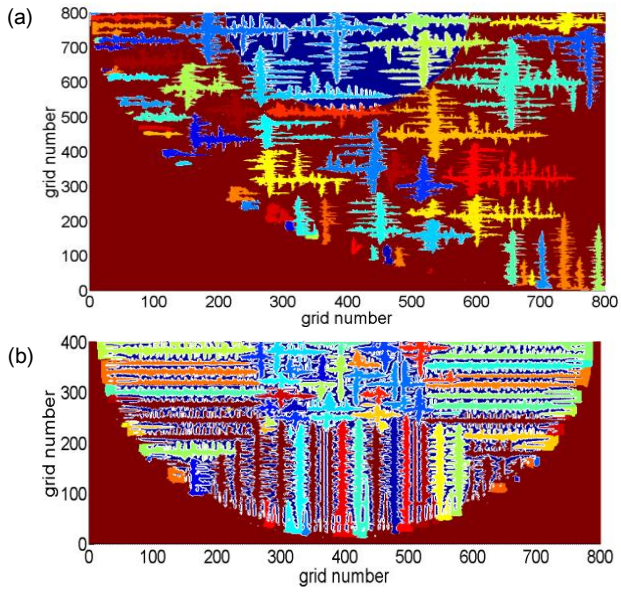

Fig. 2. The morphology of grains in the weld pool, (a) Ti-6%Al, (b) Ti-45%Al.

Copyright © 2018 VBRI Press

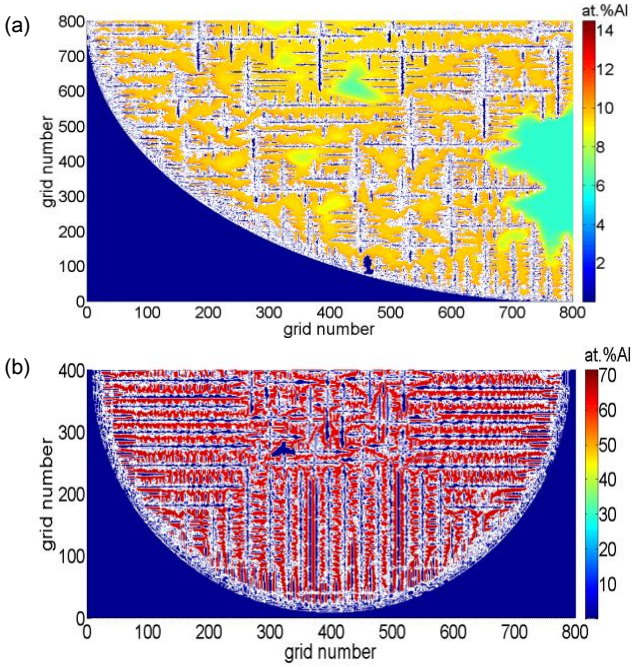

Fig. 3. The distribution of liquid solute concentration in the weld pool, (a) Ti-6%Al, (b) Ti-45%Al.

The **Fig. 3 (a,b)** show the liquid solute concentration with Ti-Al alloys of different at.%Al after the CET is over. From the **Fig. 3 (a,b),** it can be found that the columnar crystals which are close to the equiaxed crystals are due to absorbing the discharged solutes during the growth process of equiaxed crystals, thereby that leads to the rapidly rising of liquid solute concentration and the decreasing of the grow speed at the dendritic tip.

When the CET transformation is carried out in the final stage, the equiaxed crystals grow well. The solid solute concentration of Ti-6%Al reaches to 14%, while the solid solute concentration of Ti-45%Al reaches to 70%. It should be noted that the growth of the columnar crystals is completely impaired by equiaxed crystals. In addition, the competitive growth is more and more intense; the higher dendrite arm is gradually increased and roughened with solute diffusion space getting smaller and smaller and the solute concentration increasing continuously.

The **Fig. 4 (a,b)** show the solid solute concentration with Ti-Al alloys of different at.%Al after CET. On the basis of the **Fig. 4 (a,b)**, it can be obtained that the growth of dendrite is always followed by the segregation phenomenon in solid phase during the process of CET transformation. The solid phase solute concentrations of the columnar crystals and equiaxed crystals of Ti-6%Al and Ti-45%Al are the lowest respectively and the distribution is about 3% and 5%, which is lower than the initial solute concentration. It can be found that the concentration of solid solute in the equiaxed crystal and columnar crystal tip is the highest, which is due to ingredient undercooling and curvature undercooling. It is easy to form regional segregation after solidification. Hence, the evolution of columnar-equiaxed crystals is not only the columnar crystals being hindered by the equiaxed grains, but also the interaction between the solid and liquid solute concentrations.

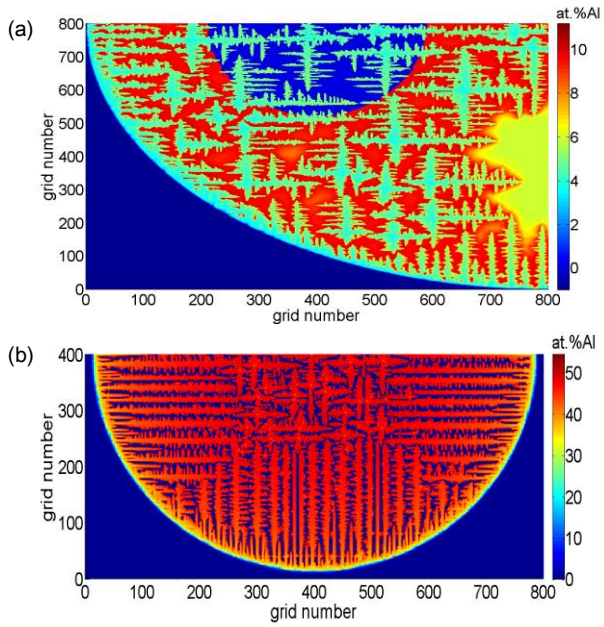

Fig. 4. The distribution of solid solute concentration in the weld pool, (a) Ti-6%Al, (b) Ti-45%Al.

The **Fig. 5 (a,c)** describe that the metallographic experiments of Ti-6%Al and Ti-45%Al in the molten pool, also the simulations of Ti-6%Al and Ti-45%Al in the welding pool. The columnar crystals grow from the vicinity of the fusion line and extend to the center of the weld. Simultaneously, in the center of molten pool the equiaxed organization also is formed. Moreover, the quantity of the equiaxed dendrites is well above the columnar dendrites for Ti-6%Al as well as the quantity of the columnar dendrites is much more than the equiaxed dendrites in the molten pool for Ti-45%Al. Compared the simulated results with the experimental ones, the rationality and accuracy of the model established are verified. The β phase and α phase are produced in solidification process. It can be concluded that the above simulated results are in good agreement with the experimental results about the directional research of dendritic morphology.

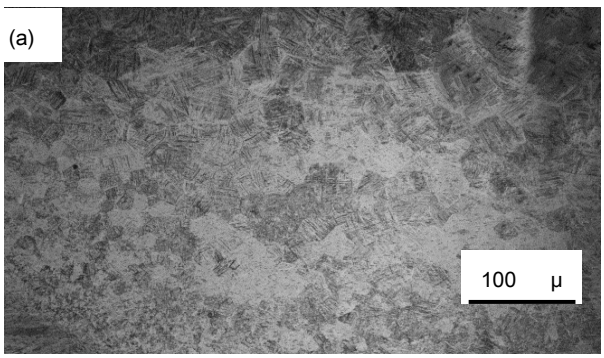

Copyright © 2018 VBRI Press

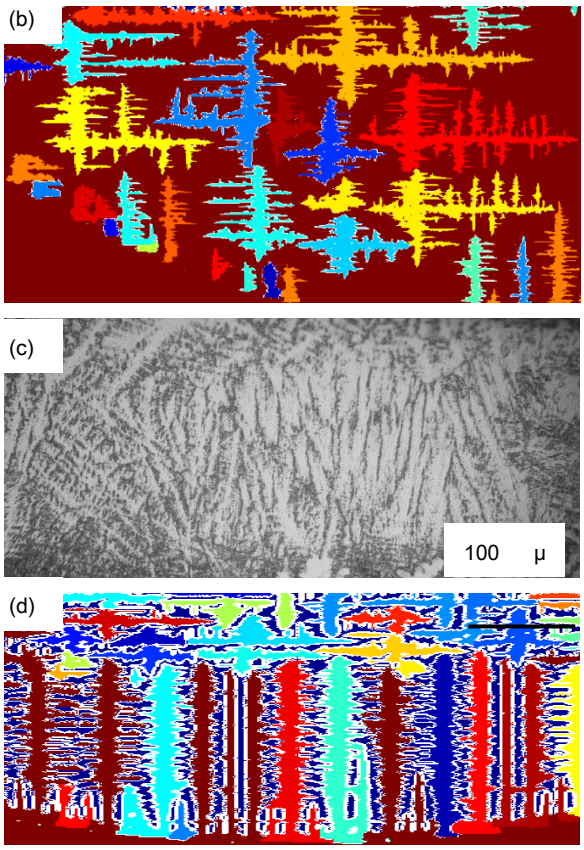

Fig. 5. Micrographs of Ti-6%Al and Ti-45%Al alloy in the welding pool, (a, c) experimental results, (b, d) simulated results.

Discussion

Firstly, it should be pointed that the simulated results are in good agreement with the experimental ones for the directional study of dendritic morphology. However, there is a certain error in the preferred orientation of the dendrites between the simulated results and the simulated results. Therefore, the model needs to be further improved and the number of grains also needs to be quantified in the future work.

Conclusion

The thermal process of welding and the dendritic growth process of molten pool for Ti-6%Al and Ti-45%Al in TIG welding are simulated by means of the finite difference method and the CA method. The following conclusions are obtained:

1) The solute atoms are enriched in between dendrite arms with the segregation of solute.
2) The temperature at the center of the molten pool presents the gradual distribution in the non-uniform temperature field. With the change of temperature field, the dendrites have inconsistent morphology.
3) The change of Al initial composition for Ti-Al alloys has a great effect on dendritic morphologies during the process of CET.
4) In the oriented research of dendritic morphology, the simulation is in a good accordance with that of the experimental results.

Acknowledgements

The authors gratefully acknowledge the financial support from Natural Science Foundation of China (Grant No.51274162), Education Department of Shaanxi Provincial Government scientific research projects of key laboratory (Grant No.15JS082), Education Department of Shaanxi Provincial Government service local special projects (Grant No.16JF021).

Author's contributions

Conceived the plan: MZ; Performed the experiments: YLZ, ELM; Data analysis: YLZ, QX; Wrote the paper: YLZ. Authors have no competing financial interests.

Supporting information

Supporting informations are available from VBRI Press.

References

1. Zhao, B.; Wang, H.; Qiao, N.; et al.; *Mater. Sci. Eng. C*, **2017**, *70*. **DOI:** 10.1016/j.msec.2016.07.045
2. Machethe, K.E.; Popoola, A.P.I.; Adebiyi, D.I.; et al.; Pro. Mfg., **2016**, *7*. **DOI:** 10.1016/j.promfg.2016.12.069
3. Jung, I.S.; Kim, M.C.; Lee, J.H.; et al.; *Intermet.*, **1999**, *7*, 11. **DOI:** 10.1016/S0966-9795(99)00031-X
4. Barbosa, J.; Ribeiro, C.S.; Monteiro, A.C.; *Intermet.*, **2007**, *15*, 7. **DOI:** 10.1016/j.intermet.2006.11.004
5. Arenas, M.F.; Acoff, V.L.; *Scr. Mat.*, **2002**, *46*, 3, 1. **DOI:** 10.1016/S1359-6462(01)01232-5
6. Liu, B.C.; Xu, Q.Y.; Tsinghua Science and Technology, **2004**, *9*, 5.
7. Dong, Z.B.; Wei, Y.H.; Liu, R.H.; et al.; *China Welding*, **2004**, *13*, 1.
8. Gandin, C.A.; Rappaz M.; *Acta Metall. Et Mat.*, **1994**, *42*, 7. **DOI:** 10.1016/0956-7151(94)90302-6
9. Yin, H.; Felicelli, S.D.; Wang, L.; *Acta Mat.*, **2011**, *59*, 8. **DOI:** 10.1016/j.actamat.2011.01.052
10. Eshraghi, M.; Felicelli, S.D.; Jelinek, B.; *J. Crys. Gro.*, **2012**, *354*, 1. **DOI:** 10.1016/j.jcrysgro.2012.06.002
11. Chen, S.; Guillemot, G.; Gandin, C.A.; *Acta Mat.*, **2016**, *115*. **DOI:** 10.1016/j.actamat.2016.05.011
12. Tan, W.; Bailey, N.S.; Shin, Y.C.; Com. Mat. Sci., **2011**, *50*, 9. **DOI:** 10.1016/j.commatsci.2011.03.044
13. Tan, W.; Shin, Y.C.; *Com.Mat. Sci.*, **2015**, *98*, 10. **DOI:** 10.1016/j.commatsci.2014.10.063
14. Luo S, Zhu M Y.; *Com. Mat. Sci.*, **2013**. **DOI:** 10.1016/j.commatsci.2012.12.040
15. Zhang, X.; Zhao, J.; Jiang, H.; et al.; *Acta Mat.*, **2012**, *60*, 5. **DOI:** 10.1016/j.actamat.2011.12.045
16. Lin. H.K.; Chen, C.C.; Lan, C.W.; *J. Crys. Gro.*, **2011**, *318*, 1. **DOI:** 10.1016/j.jcrysgro.2010.11.013
17. Tang, S.; Backofen, R.; Wang, J.; *et al.; J. Crys. Gro.*, **2011**, *334*, 1. **DOI:** 10.1016/j.jcrysgro.2011.08.027
18. Zhan, X.H.; Wei, Y.H.; Dong, Z.B.; *J. Mat. Pro. Tec.*, **2008**, *208*, 1. **DOI:** 10.1016/j.jmatprotec.2007.12.130
19. Chen, J,; Zhu M.F.; Sun, G.X.; Acta Met. Sin., 2005, 41, 8.
20. Chen, J.Q.; Xiao, S.H.; Yang X.Y.; et al.; *Equip. Manu. Tech.*, **2005**.
21. Xiao, Y.H.; Zhang, H.F.; Ping, X.C.; *J. East China Jiaotong University*, **2014**, *32*.
22. Tsai, D. C.; Wang, W.S.; *Trans. Nonfe. Metal Soc. China*, **2010**, *20*, 6. **DOI:** 10.1016/S1003-6326(09)60260-0
23. Minoru, Y.; Yukinobu, N.; Hiroshi, H.; Kenichi, O.; *ISIJ International*, **2006**, *46*, 6.
24. Zhu, M. F.; Stefanescu, D.M.; *Acta Mat.*, **2007**, *55*, 5. **DOI:** 10.1016/j.actamat.2006.10.037
25. Nastac.; *Acta Met.*, **1999**, *47*,17. **DOI:** 10.1016/S1359-6454(99)00325-0
26. Beltran-Sanchez, L.; Stefanescu, D.M.; *Met. Mat. Trans. A*, **2004**, *35*.
27. Sasikumar, R.; Kumar, M. ; *Acta Met. Mat.*, **1995**, *43*, 12. **DOI:** 10.1016/0956-7151(95)00114-B

Copyright © 2018 VBRI Press